Chapter 5: Dual-Band Dual-Sense Circularly Polarized High Gain Suspended Plate Antenna for Bio-Telemetry Applications

In this chapter, we introduce a dual-band dual-sense (DBDS) high gain circularly-polarized suspended plate antenna for bio-telemetry. Operating in Wireless Medical Telemetry Service (WMTS) bands (1.395 – 1.400 GHz and 1.427 – 1.432 GHz) and the Industrial, Scientific, and Medical (ISM) band (2.48 GHz - 2.4 GHz), the antenna features a 98 mm diameter circular metallic radiator (0.45 λ at 1.4 GHz) with an L-probe feed. Electromagnetic coupling between feeding strips and a center slot broadens the impedance bandwidth. Dual-band circularly polarized operation incorporates specific features for both the WMTS and ISM bands, utilizing notches for WMTS and slot loading on a circular patch dedicated to the ISM band. The prototype undergoes fabrication and measurement, revealing impressive metrics. Simulation results show an 11.42% impedance bandwidth (1.42 GHz - 1.26 GHz) for the WMTS band and a 37.55% bandwidth (2.95 GHz - 2.03 GHz) for the ISM band. Measured bandwidths are 15% (1.44 GHz - 1.23 GHz) for the WMTS band and 34.6% (2.93 GHz - 2.08 GHz) for the ISM band. Measured peak gain is 8.9 dBi at 1.4 GHz and 10.15 dBi at 2.45 GHz. The measured 3dB axial ratio bandwidth is 5.7% (1.41 GHz - 1.33 GHz) for the WMTS band and 11% (2.59 GHz - 2.32 GHz) for the ISM band. The antenna achieves right-hand circular polarization (RHCP) for the WMTS band and left-hand circular polarization (LHCP) for the ISM band, as confirmed through measurements. Validation with a dual-band ingestible antenna demonstrates the proposed antenna's success in reducing polarization mismatch, maintaining reliable communication links, highlighting its potential in dual-band bio-telemetry systems.*

---

*Part of this chapter have been published: Dubey, & Meshram, M. K. (2023). Dual-Band Dual-Sense Circularly Polarized Suspended Plate Antenna with L-Probe Feed for Biotelemetry Application. *IEEE Transactions on Antennas and Propagation*, (Under review).

5.1 Introduction

Biotelemetry applications are transforming healthcare by enabling real-time monitoring of vital signs and minimally invasive treatments. Reliable wireless communication is crucial for transmitting critical medical data from implanted and wearable devices [109]-[112]. However, efficient data transfer can be hindered by multipath fading and polarization mismatch. Circularly polarized (CP) antennas offer a promising solution to mitigate these challenges by providing constant signal strength and eliminating the need for precise antenna alignment [113]-[114]. This characteristic is particularly valuable for implantable devices and on-body sensors, where accurate data transmission is crucial for patient well-being. Fig. 5.1: Illustrating a biotelemetry application where an ingestible/implantable wireless capsule transmits vital signs data to an external receiver for remote patient monitoring

CP antennas combat polarization mismatch, but biotelemetry demands multi-band operation due to diverse device needs. MICS/MedRadio (402-434 MHz) serve implants [115]-[122] and medical telemetry, while WMTS (1.395-1.432 MHz) monitors vital signs [123]-[125]. ISM bands (915 MHz, 2.45 GHz) cater to wearables and WBANs, offering favourable propagation and regulatory benefits [125]-[132]. Thus, multi-band antennas are crucial for seamless biotelemetry across diverse devices and sensors.

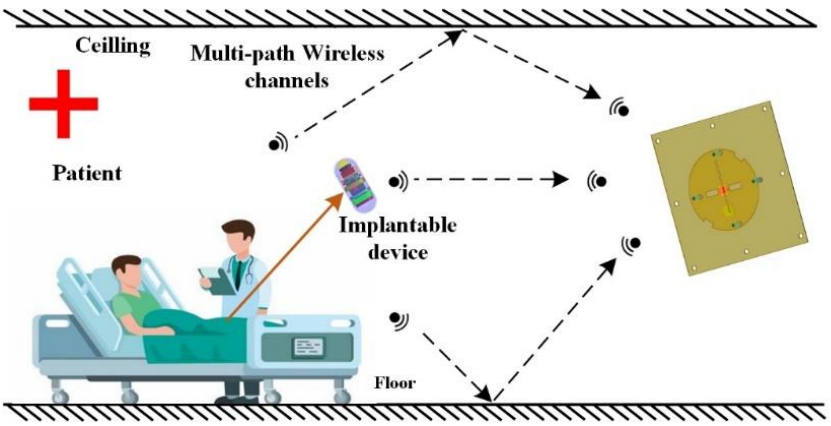

Fig. 5.1: An application of biotelemetry system (AI-generated base, edited in Microsoft Visio).

Furthermore, dual-band dual-sense CP antennas offer an additional advantage by providing two orthogonal CP modes with the same frequency and polarization sense [133],[80]-[91]. In [133] introduces a dual-band CP antenna on a circular substrate, demonstrating commendable axial ratios without ground plane perturbation. The feeding technique involves V-shaped resonators, contributing to miniaturization. Compact microstrip arrays with non-radiating resonators, as presented in [80], enable scalable arrays with uniform gain. The feeding technique involves a single-layer configuration, emphasizing simplicity and ease of integration. In [81], a low-profile switchable CP patch antenna achieves selectable RHCP/LHCP states in both bands through shared feeding networks and SPST switches. The feeding technique involves shared feeding networks, emphasizing a practical and compact implementation. The metasurface antenna outlined in [82], leveraging characteristic mode analysis, attains high gain and wide axial ratio bandwidths. The feeding technique involves coupled-fed slots, suppressing unwanted modes for enhanced performance. Reference [83] contributes a dual-band CPW-fed monopole with parasitic elements for wide bandwidths. The antenna design comprises a single layer, emphasizing simplicity, and the feeding technique involves CPW. Additionally, [87] proposes a CPW-fed slot antenna with a C-shaped grounded strip, providing tunable axial ratio bandwidths. The antenna design involves a single layer with CPW feeding. Multiple bands and switchable CP bands are addressed by [88] through magnetoelectric dipole structures and by [91] via reactively loaded annular slots.

Amid the potential of dual-band dual-sense CP antennas to significantly enhance biotelemetry performance, suspended plate antennas emerge as promising candidates due to their inherent high-gain characteristics. These antennas, utilizing a conductive plate suspended above a ground plane, create a resonant cavity with efficient energy confinement and radiation [92],[134]-[136].

However, limited studies have explored the potential of suspended plate antennas for achieving dual-band dual-sense circular polarization for high Gain. Addressing this research gap, our study focuses on the novel concept of a Dual-Band Dual-Sense Circularly Polarized Suspended Plate Antenna (DBDS CP SPA) designed specifically for biotelemetry. Leveraging Characteristic Mode (CM) theory, a powerful tool for analyzing antennas of arbitrary shapes, our research provides valuable insights into the intrinsic resonant behaviour of the proposed design [137]-[140].

We introduce a novel DBDS CP SPA with an L-probe feed, tailored for operation in the Wireless Medical Telemetry Service (WMTS) bands (1.395–1.400 GHz and 1.427–1.432 GHz) and the Industrial, Scientific, and Medical (ISM) band (2.48–2.4 GHz). This addresses the need for dual-band communication in the biomedical field. The antenna features a circular metallic radiator with a 98 mm diameter (0.45 λ at 1.4 GHz), ensuring optimal performance in the targeted frequency bands.

The integration of CM theory for mode analysis and the L-probe feed for dual-sense CP operation represents novel approaches in biotelemetry antenna design. The feeding mechanism, comprising double L-shaped strips, and the electromagnetic coupling between these strips and the centre slot contribute to a broad impedance bandwidth. Strategically placed indentations and slot loading on the circular patch enable dual-band circularly polarized operation.

The fabricated prototype undergoes rigorous measurement and simulation, demonstrating impressive impedance bandwidths, peak gains, and axial ratio bandwidths in both the WMTS and ISM bands. These results collectively affirm the effectiveness of the proposed DBDS CP SPA in meeting the specific requirements of biotelemetry applications. Subsequent sections delve into the design methodology, simulation results, experimental validation, and a comprehensive analysis of the antenna's performance in both frequency bands.

5.2 Antenna Configurations

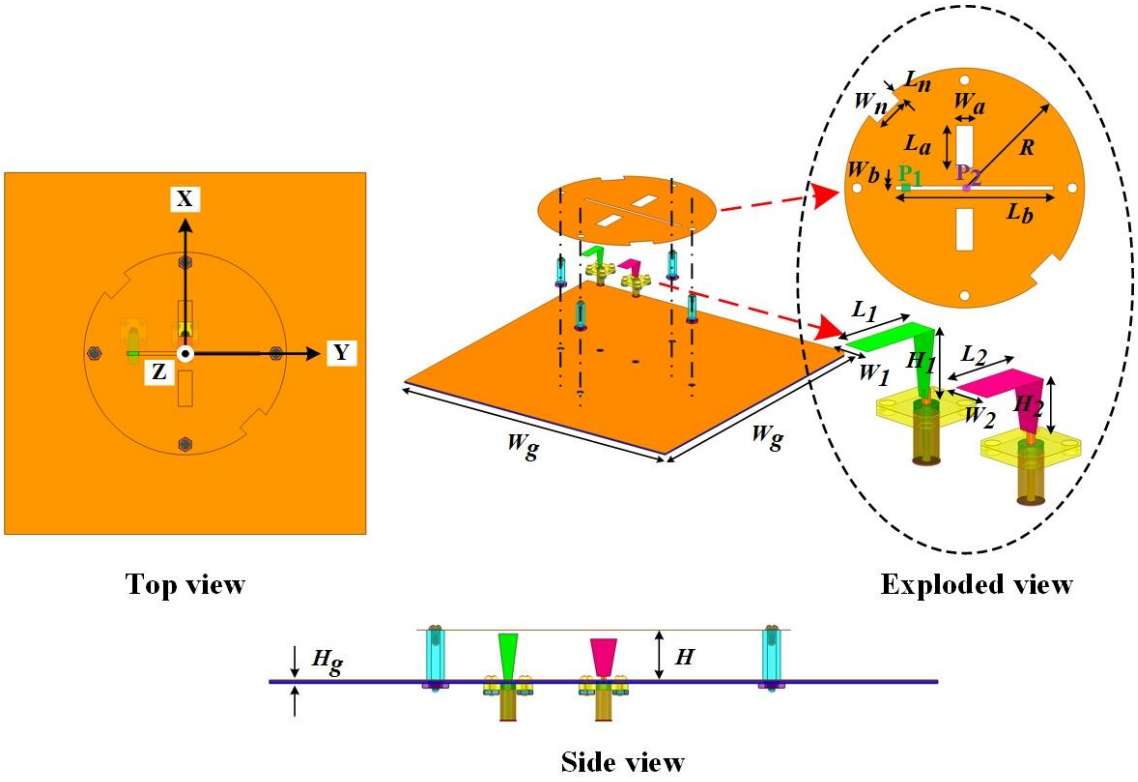

Fig. 5.2: Geometry of the proposed DBDS suspended plate CP antenna

The proposed dual-band dual-sense circularly polarized (DBDS CP) suspended plate antenna, illustrated in Fig.5.2, comprises a radiating circular plate, a ground plane, and an L-shaped probe feed. This antenna configuration is defined within a coordinate system, aligning the radiating circular plate in the XY plane with its Z-axis vertically centered through the structure. This deliberate orientation ensures symmetrical characteristics along both the X and Y axes, a crucial aspect of the antenna's design.

An exploded view of Fig.5.2 reveals the antenna's geometric parameters and detailed specifications for the feeder. Through extensive numerical simulations conducted using CST Microwave Studio software, the antenna's geometric parameters were optimized, yielding the values presented in Table 5.1. From a side view, the radiating patch of the antenna is strategically positioned at a height (H) of 13.2 mm above a ground plane. The

copper patch, circular in shape with a radius of R (49 mm), is constructed using a 1 mm thick copper sheet.

Table 5.1: Dual-band dual-sense circularly polarized (DBDS CP) suspended plate antenna Parameters

Parameter	Value (in mm)	Description
W_g	175	Ground plane width
H_g	*0.8*	Ground plane thickness
H	*13.2*	Radiator height above the ground
W_n	*9.2*	Inset slit width
L_n	*4.56*	Inset slit length
W_a	*6.9*	Small rectangular slot width
L_a	*17.28*	Small rectangular slot length
R	*49*	Patch radius
W_b	1.72	Narrow rectangular slot width
L_b	64.6	Narrow rectangular slot length
L_1	15.0	Horizontal arm length port#1
W_1	6.9	Horizontal arm width port#1
H_1	12.2	Vertical arm length port#1
L_2	12.6	Horizontal arm length port#2
W_2	6.9	Horizontal arm width port#1
H_2	11.6	Vertical arm length port#1

As depicted in the exploded view of Fig. 5.2, a narrow rectangular slot (L_b X Wb = 64.6 mm X 1.72 mm) is centrally cut into the plate, with its longer sides parallel to the Y-axis. Additionally, two small rectangular slots (L_a X W_a = 17.28 mm X 6.9 mm) are placed orthogonally to the narrow slot. The L-shaped probe features vertical arm lengths H_1 and H_2 of 12.2 mm and 11.6 mm, respectively, and horizontal arm lengths L_1 and L_2 of 15 mm and 12.6 mm, respectively. The probe's horizontal arm is positioned near the edge of the rectangular slot at P1 and at the center of the slot at P2. The L-shaped probe feeding structure comprises horizontal arm width port#1 and horizontal arm width port#2 wide strips of dimensions W_1 and W_2, both 6.9 mm. A square-shaped ground plane copper plate with dimensions W_g (175 mm) serves as the ground plane. The radiating circular patch is supported by four acrylic plastic poles.

5.2.1 Characteristic Mode Theory for DBDS CP Antenna

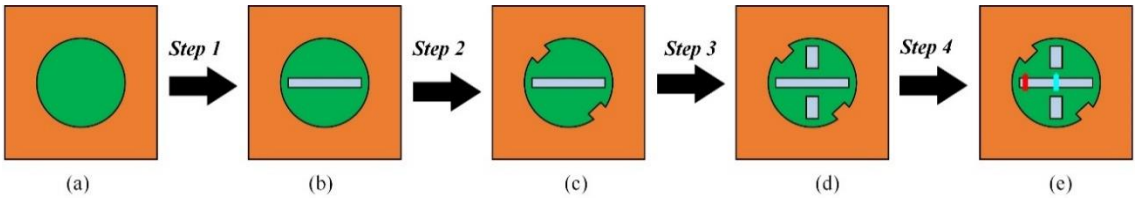

Fig. 5.3: Antenna evolution using CMA of a DBDS CP antenna

The evolution of the DBDS CP antenna design is depicted in Fig.5.3. The initial design (Stage 1) employed a fundamental suspended circular plate antenna, providing a baseline for subsequent modifications. Stage 2 introduced a simple slot, followed by the insertion of additional slits in Stage 3, both aimed at enhancing dual-band dual-sense circularly polarized (DBDS CP) performance. Stage 4 further optimized the design by incorporating orthogonal slot loading. These progressive modifications culminated in the final antenna (Stage 5), exhibiting significantly improved DBDS CP characteristics compared to the initial design.

5.2.1.1 Stage 1: Suspended Circular Plate Antenna

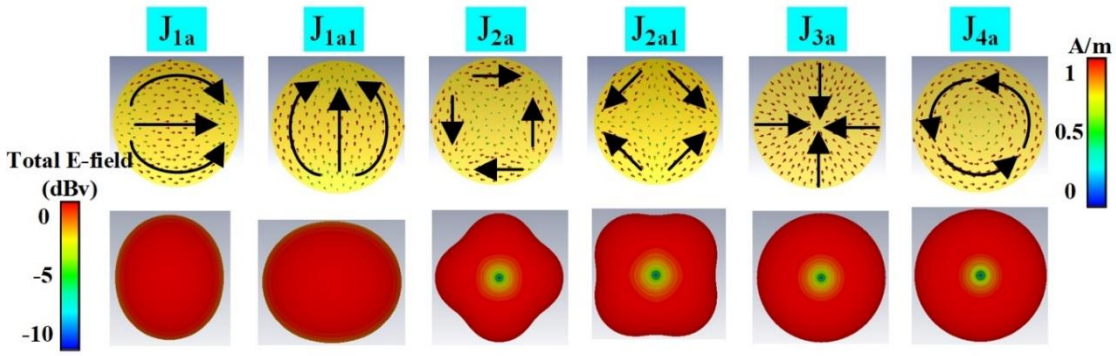

(a)

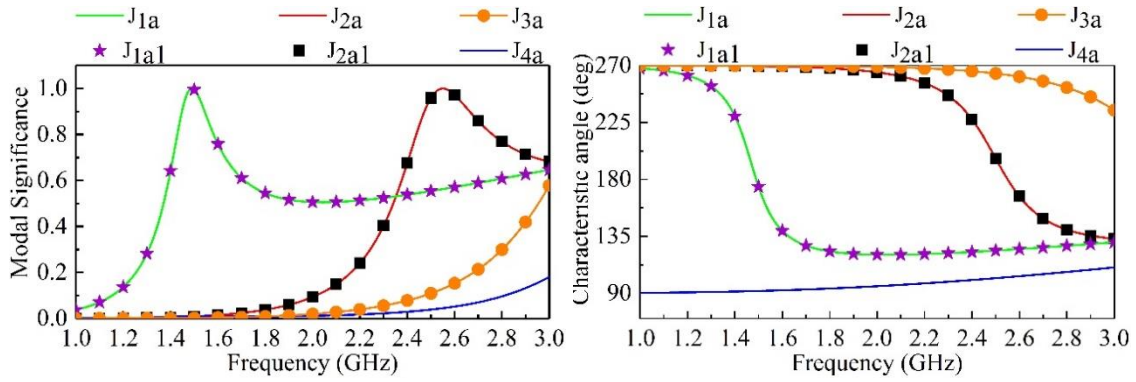

(b) (c)

Fig. 5.4: Suspended Circular Plate Antenna (a) Modal significance's corresponding modal current, and corresponding radiation pattern (b) Modal significance, and (c) Characteristic angle

Modal analysis of the initial suspended circular plate antenna (Stage 1, Fig. 5.3) reveals six dominant modes influencing its radiation characteristics: J1a, J1a1, J2a, J2a2, J3a, and J4a. Interestingly, both J1a/J1a1 at 1.4 GHz and J2a/J2a2 at 2.45 GHz exhibit degeneracy, potentially leading to unique interactions and distinct radiation patterns. J1a and J1a1 contribute to broadside radiation in the far-field due to their orthogonal in-phase currents. Conversely, despite high modal significances, J2a, J2a2, J3a, and J4a suffer from undesirable null points in the boresight region, impacting potential gain and directivity. However, the higher resonant frequencies of J3a and J4a offer an opportunity for extending the antenna's operational bandwidth. Optimizing their radiation patterns to mitigate the

boresight nulls remains crucial for achieving optimal performance. This initial analysis sets the stage for subsequent modifications aimed at mitigating the detrimental effects of certain modes and harnessing the potential of higher-order resonances for broader bandwidth.

5.2.1.2 Stage 2: Modified Suspended Circular Plate Antenna with Slot

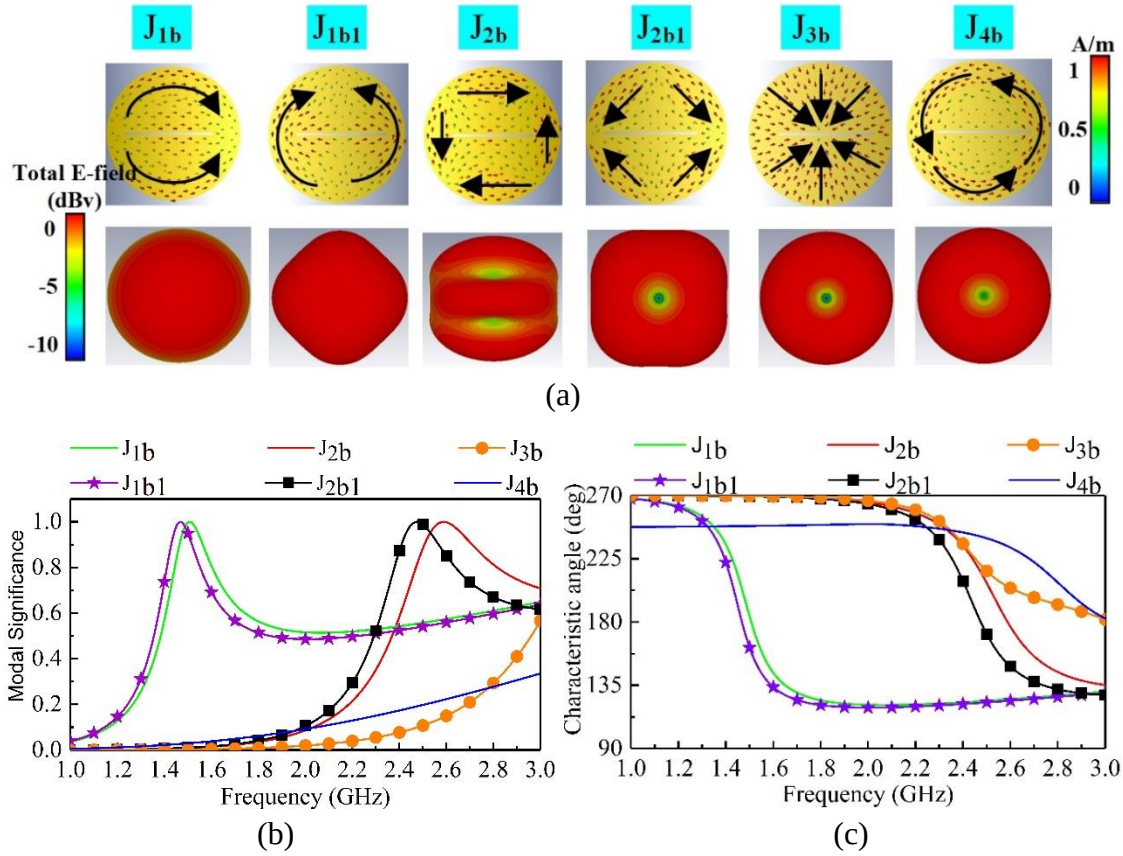

Fig. 5.5: Modified Suspended Circular Plate Antenna with Slot (a**)** Modal significance's corresponding modal current, and corresponding radiation pattern (b) Modal significance, and (c) Characteristic angle

The introduction of a narrow rectangular slot in Stage 2, as depicted in Fig. 5.3, significantly perturbs the antenna's modal landscape. The corresponding modal significances, currents, and radiation patterns are presented in Fig. 5.5. This modification disrupts the degeneracies of J1b/J1b1 at 1.4 GHz and J2a/J2a2 at 2.45 GHz, leading to frequency shifts for J1b1 and J2a2 due to their elongated surface current paths. While J3b and J4b remain largely unaffected due to their low modal significances, the slot positively

influences the radiation patterns as shown in Fig. 5.5(a). J1b and J1b1 at 1.4 GHz continue to exhibit desirable broadside radiation, while J2a, J2a2, J3b, and J4b retain null points in the broadside pattern, potentially impacting gain and directivity (Fig. 5.5(a)).

5.2.1.3 Stage 3: Further Modified Suspended Circular Plate Antenna with Inserted Slits

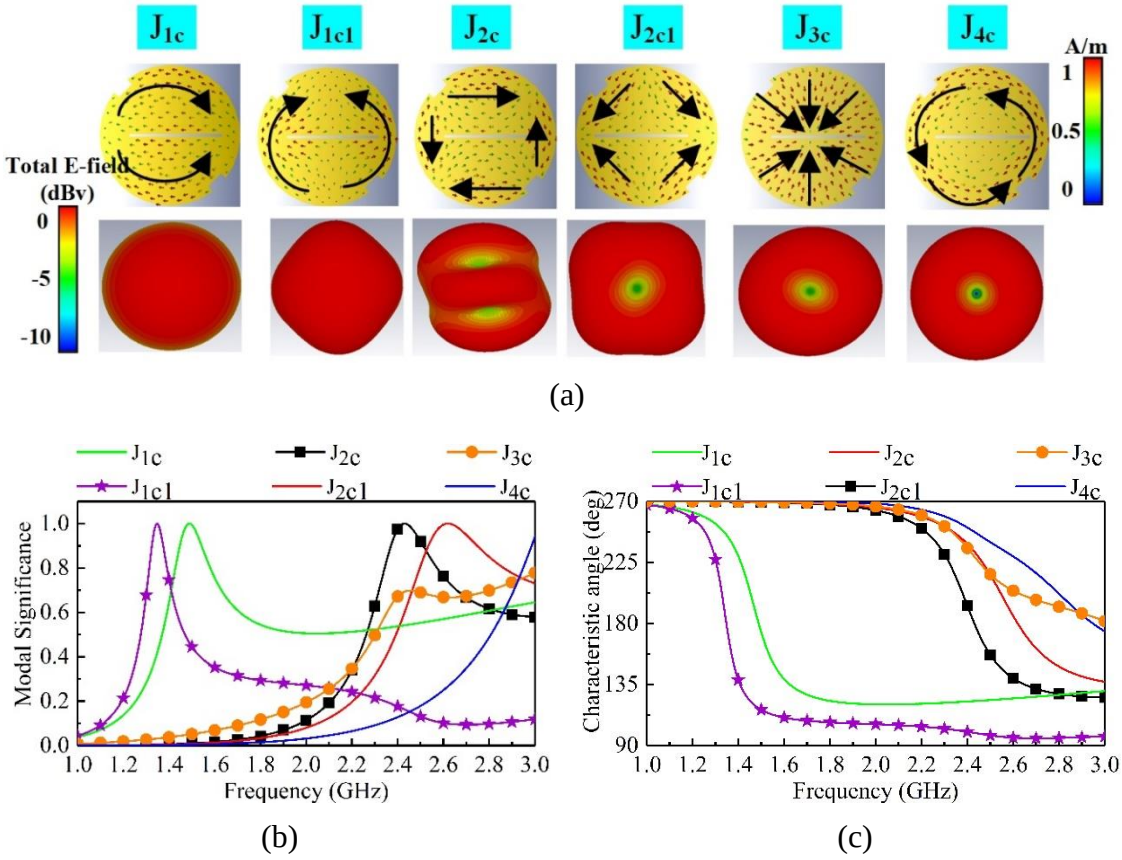

Fig. 5.6: Modified Suspended Circular Plate Antenna with Inserted Slits (a) Modal significance's corresponding modal current, and corresponding radiation pattern (b) Modal significance, and (c) Characteristic angle

In Stage 3, the integration of inserted slits into the suspended circular plate antenna introduces further alterations to the modal landscape, as presented in Fig. 5.6. Notably, these slits successfully perturb the degeneracy of J1c/J1c1 at 1.4 GHz. Crucially, the characteristic angle between these modes approaches 90 degrees (Fig. 5.6(c)), a condition essential for achieving circular polarization. While the modal significances of J2a and J2a2 at 2.45 GHz are also perturbed (Fig. 5.6(b)), their characteristic angle does not reach the

threshold for circular polarization, suggesting potential for further optimization. The radiation patterns associated with J2c, Jc1, J3c, and J4c, as depicted in Fig. 5.6(a), continue to exhibit null points in the broadside direction, indicating a need for additional modifications to enhance gain and directivity in those modes.

5.2.1.4 Stage 4: Further Modified Suspended Circular Plate Antenna with Orthogonal Slot Loading

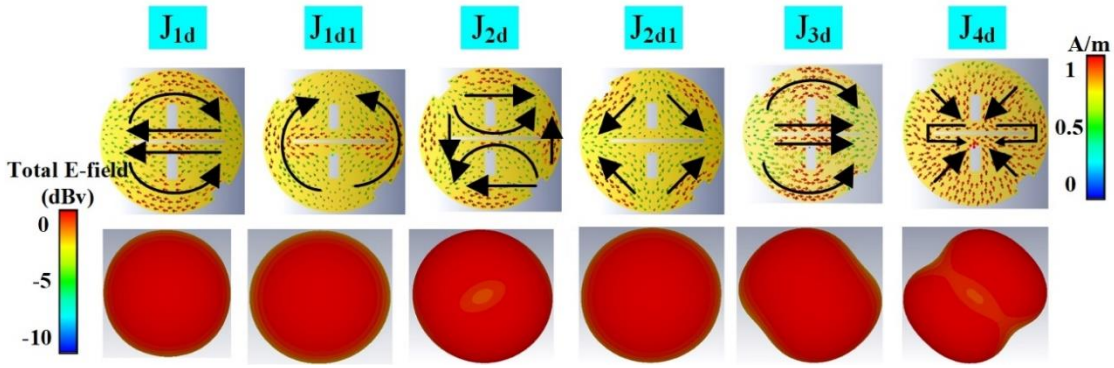

(a)

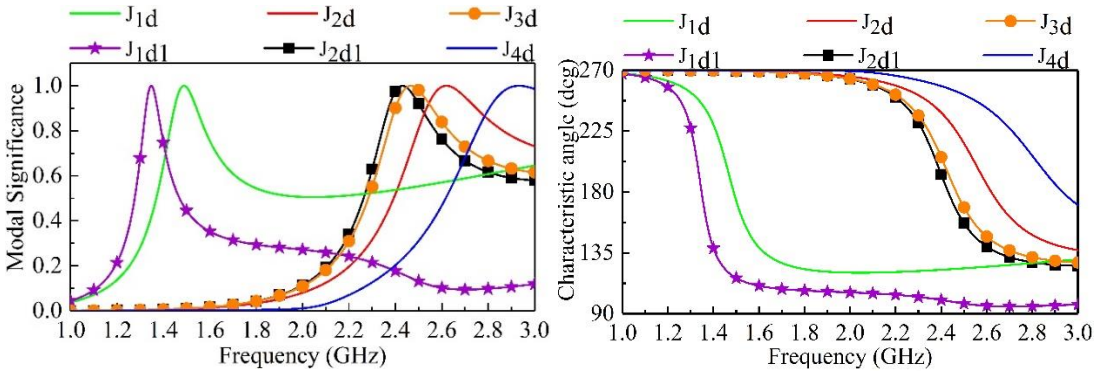

(b) (c)

Fig. 5.7: Modified Suspended Circular Plate Antenna with Orthogonal Slot Loading (a) Modal significance's corresponding modal current, and corresponding radiation pattern (b) Modal significance, and (c) Characteristic angle

In Stage 4, the implementation of orthogonal slot loading in the suspended circular plate antenna, as illustrated in Fig. 5.7, produces a distinct set of modal interactions and radiation characteristics. While the modal significances of J1d/J1d1 at 1.4 GHz remain largely

unaffected, the loading significantly perturbs J2d and J2d2 at 2.45 GHz. Importantly, the characteristic angle between these modes achieves a near-90-degree separation (Fig. 5.7(c)), fulfilling the critical condition for circular polarization. Furthermore, J3d and J4d exhibit pronounced modal significances at 2.6 GHz and 2.8 GHz, respectively (Fig. 5.7(b)), suggesting potential for bandwidth extension. Notably, the radiation patterns associated with J2d, J2d2, J3d, and J4d (Fig. 5.7(a)) demonstrate the successful elimination of null points in the broadside direction, leading to enhanced gain and directivity in these modes.

5.2.1.5 Stage5: Implementing DBDS CP performance

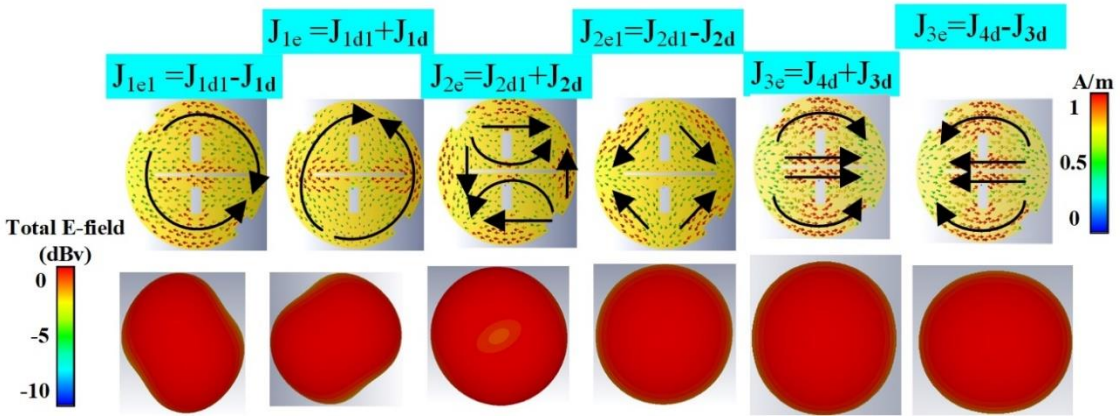

(a)

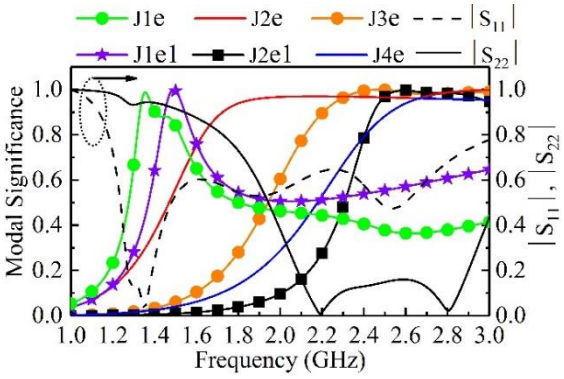

(b)

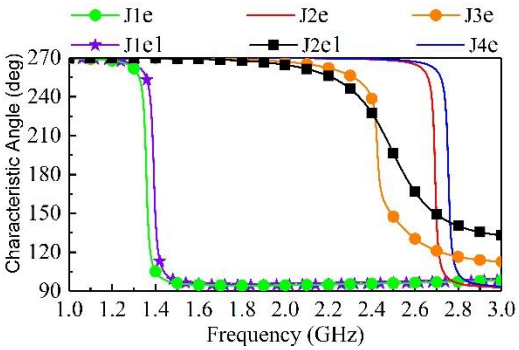

(c)

Fig. 5.8: Implementing DBDS CP performance (a) Modal significance's corresponding modal current, and corresponding radiation pattern (b) Modal significance, and (c) Characteristic angle.

The final design stage involves strategic selection of feed positions P1 and P2 to excite the suspended plate antenna, as shown in Fig. 5.8. The result-driven model analysis, including modal significances and reflection coefficients (Fig. 5.8(b)), demonstrates successful excitation of desired modes and achievement of circular polarization across multiple frequency bands. Notably, broadside modes J1e1 and J1e, characterized by surface currents along and orthogonal to the slit (Fig. 5.8(a)), exhibit a near-90-degree characteristic angle difference (Fig. 5.8(c)). This difference arises from the -45 degree and +45degree phase shifts associated with J1d1-J1d and J1d1+J1d, respectively, leading to right-hand circular polarization (RHCP) in the lower band at 1.4 GHz. Similarly, modes J2e and J2e1, formed by combining J2d1 and J2d, achieve a 90-degree characteristic angle difference at 2.45 GHz, resulting in left-hand circular polarization (LHCP). This pattern repeats for modes J3e and J3e1, formed by J4d and J3d, at 2.7 GHz, further extending the LHCP band.

5.2.2 Parametric Analysis

The numerous design variables within the suspended plate antenna necessitate a comprehensive parametric study for optimal performance. An L-shaped probe excites a long, narrow rectangular slot, and critical dimensions La, Lb, L1, and L2 significantly affect antenna characteristics. These parameters require careful optimization to achieve a dual-band dual-sense circularly polarized (DBDSCP) antenna with good performance. Characteristic mode analysis (CMA) reveals a crucial insight: La and Lb primarily determine the axial ratio (AR) at the lower and higher operating bands, respectively, while L1 and L2 mainly influence the S-parameters. We conducted a parametric study on S-parameters and AR, varying one parameter at a time while keeping the optimized L-shaped feed dimensions (W1, W2, H1, and H2) constant.

5.2.2.1 The Effects of L_1

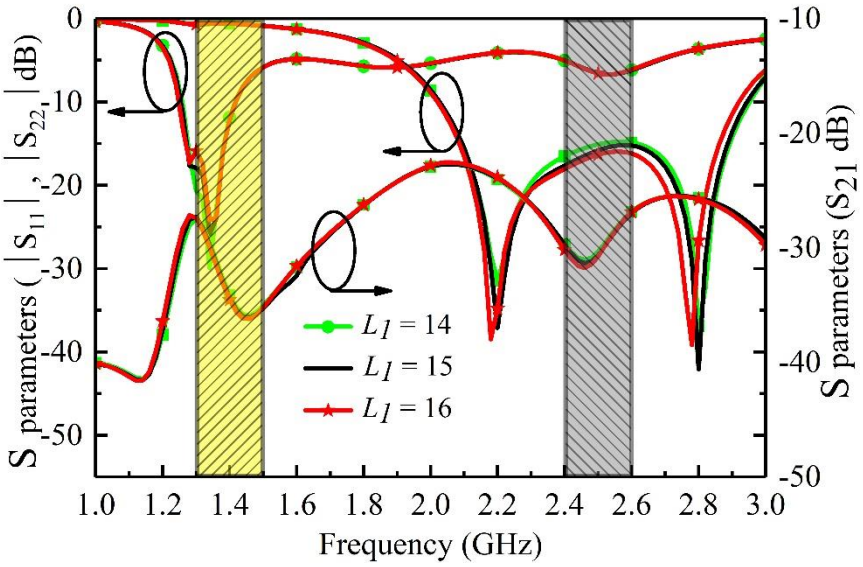

(a)

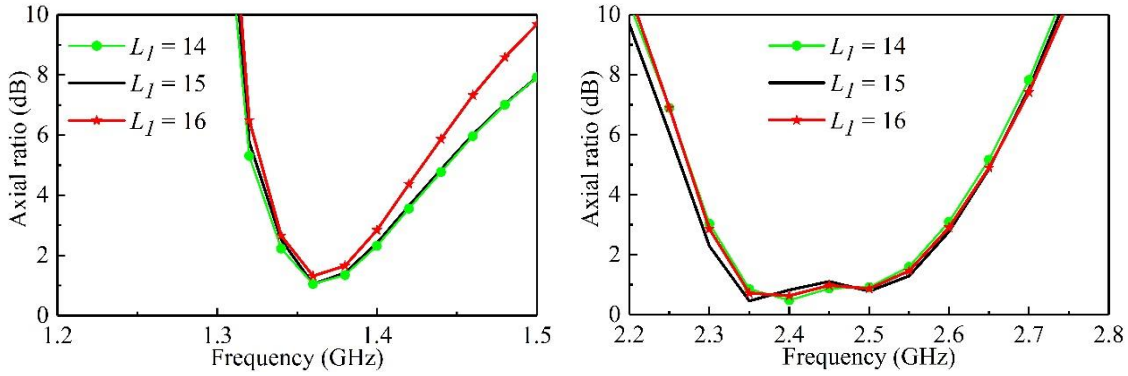

(b)

Fig. 5.9: Effect of L_1 variations on simulated (a) S-parameters and (b) axial ratio against frequency.

The impact of varying L_1 on the antenna's S-parameters and axial ratio is illustrated in Fig.5.9. As observed, L_1 minimally affects the S-parameters across both bands. However, it significantly affects the axial ratio, primarily at the lower WMTS frequency, while exhibiting negligible influence at the higher ISM band. This behaviour suggests a specific capacitive coupling between L_1 and the central narrow slot, which predominantly affects the WMTS band's axial ratio.

5.2.2.2 The Effects of L_2

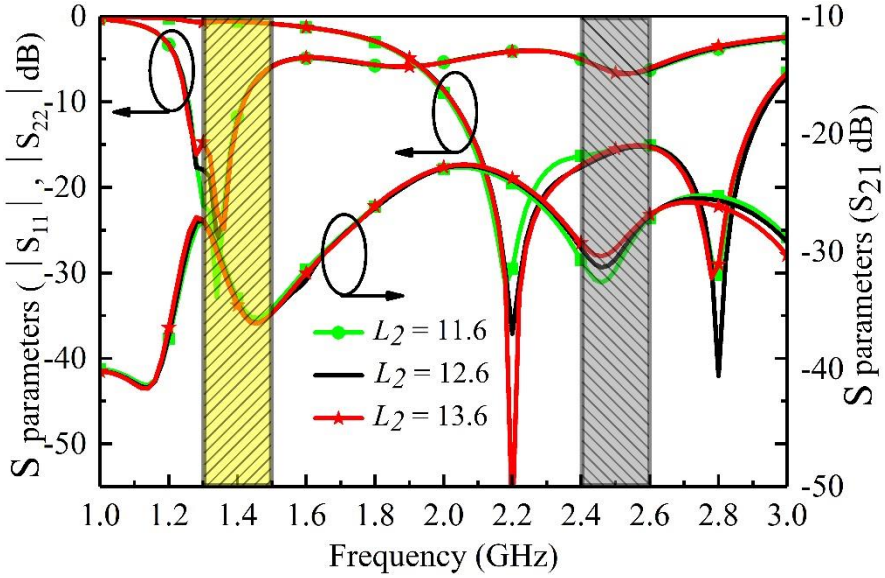

(a)

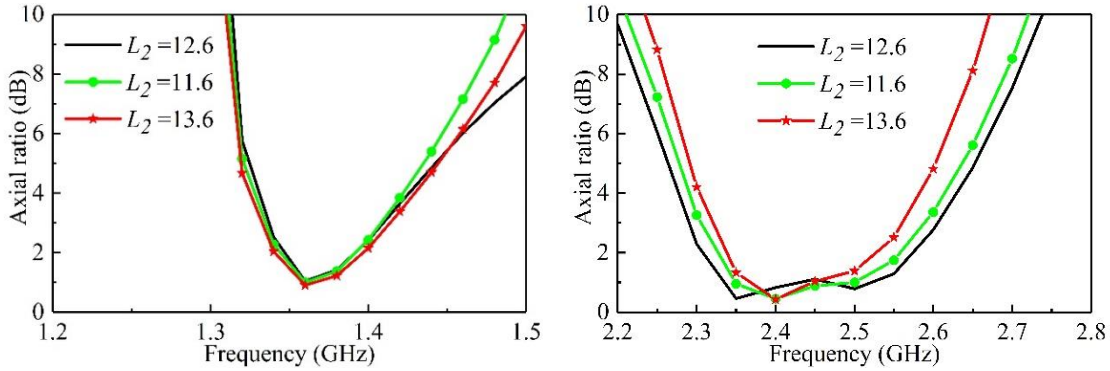

(b)

Fig. 5.10: Effect of L_2 variations on simulated (a) S-parameters and (b) axial ratio against frequency.

Following the trend observed with L_1, variations in L_2 also exhibit minimal impact on the S-parameters across both bands (Fig. 5.10). As depicted in Fig. 5.10, L_2 shows a similar trend to L_1, exerting minimal influence on the S-parameters across both bands. However, its impact on the axial ratio becomes evident at a higher frequency, primarily affecting the Industrial, Scientific, and Medical (ISM) band while demonstrating negligible influence on the lower Wireless Medical Telemetry Service (WMTS) band. This behaviour suggests a specific coupling between L_2 and the antenna elements, but at a resonance frequency distinct from

that of L_1. This observation further reinforces the notion of specific coupling between these parameters and the central narrow slot, uniquely impacting each frequency band.

5.2.2.3 The Effects of L_a

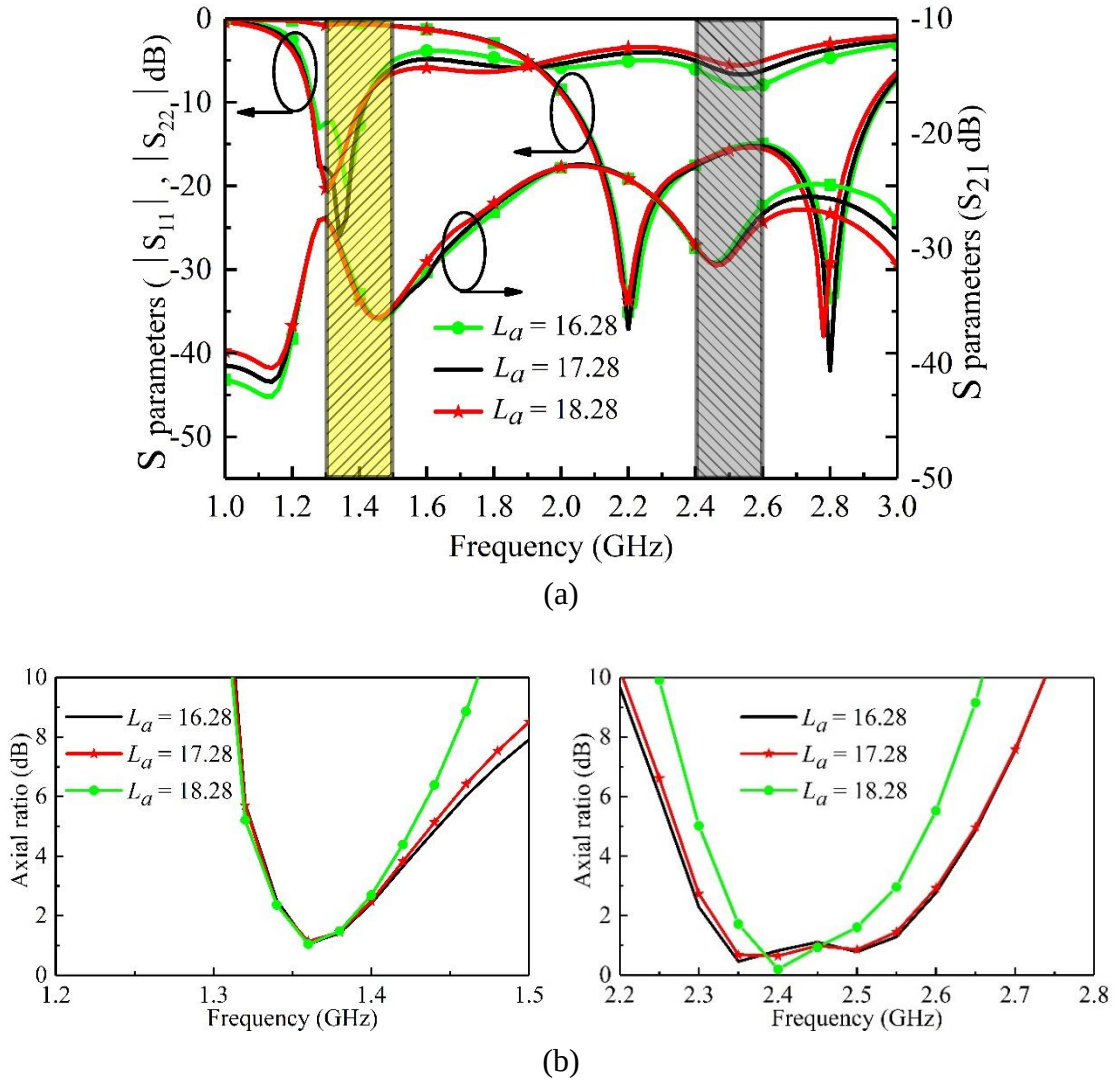

Fig. 5.11: Effect of L_a variations on simulated (a) S-parameters and (b) axial ratio against frequency.

The impact of varying the small rectangular slot length, L_a, on the antenna's performance is explored in Fig. 5.11. L_a demonstrably alters S_{11} within the lower WMTS band, exhibiting noticeable variations but exhibiting minimal impact on the higher ISM bands (Fig. 5.11(a)). This behavior suggests a specific resonance mechanism tied to L_a, primarily influencing the antenna's input impedance within the WMTS range compared to the ISM range.

As depicted in Fig. 5.11(b), it exerts a notable effect on the axial ratio, particularly at the higher ISM band compared to its minimal influence on the lower WMTS band. This distinct behavior implies that La interacts differently with the antenna elements at each resonant frequency, potentially arising from its unique influence on slot currents and field distributions within the small rectangular slot.

5.2.2.4 The Effects of L_b

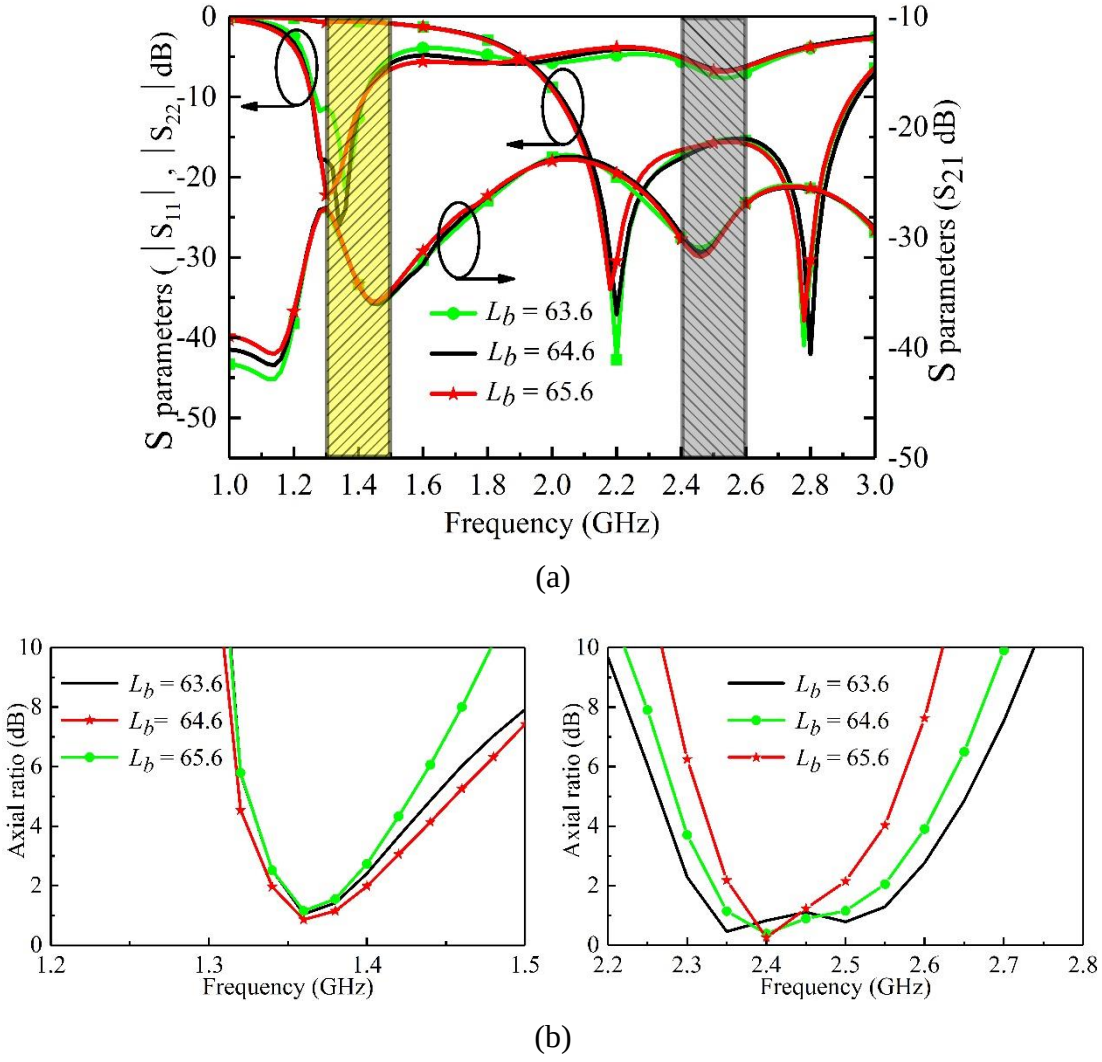

Fig. 5.12: Effect of L_b variations on simulated (a) S-parameters and (b) axial ratio against frequency.

The narrow slot length, L_b, critically shapes the antenna's performance (Fig. 5.12). It notably impacts return loss (S_{11}) in the lower WMTS band, while minimally affecting the

higher ISM band. This implies a resonance mechanism linked to L_a, primarily influencing the antenna's input impedance in the WMTS range. Conversely, L_b significantly influences the axial ratio across both bands, indicating varied interactions at each resonant frequency, potentially due to its effect on slot currents.

5.2.3 Equivalent Circuit analysis

The operational principles of the DBSC Circularly Polarized Suspended Plate Antenna are meticulously explicated through equivalent circuit analysis. Fig. 5.13(a) depicts the antenna's intricate equivalent circuit, while Fig. 5.13(b) utilizes a Smith chart to visually represent the variation in input impedance across distinct resonant frequencies. The characteristic impedance (Z_o) of the coaxial probe and the inductance (L_f) of the coaxial cable are fundamental components. A capacitive coupling between the radiating suspended plate and the L-shaped probe is facilitated by a small proximity coupling gap, denoted by capacitances C_{1g} and C_{2g} corresponding to the WMTS and ISM frequency bands.

The interconnection between L-shaped port1 and port2 is accurately modeled through resistor R_{12}, with 'p' and 's' denoting parallel and series configurations, respectively. Radiation losses are delineated by resistances R_{p11}, R_{p21}, R_{s12}, R_{p13}, R_{s12}, R_{p23}, and $R_{p24.}$ Two radiating modes, TM11 and perturbed TM21, are characterized using a combination of series and shunt resonators. For the WMTS band, the first radiating mode (TM11) is represented by a series resonator (L_{s12}, $C_{s12,}$ R_{s12}), a parallel resonator (L_{p13}, C_{p13}, R_{p13}), and a shunt tank circuit (L_{p11}, C_{p11}, R_{p11}). The second perturbed TM21 mode for the ISM band is portrayed by a series resonator (L_{s22}, C_{s22}, R_{s12}), parallel resonator (L_{p23}, C_{p23}, R_{p23}), another parallel resonator (L_{p24}, C_{p24}, R_{p24}), and a shunt tank circuit (L_{p21}, C_{p21}, R_{p21}). The essential circuit parameters for antenna functionality were extracted using Advanced Design System (ADS) and compared with results from full-wave simulation (High-Frequency Structure Simulator - HFSS) and circuit simulation, as shown in Fig. 5.13(c) and 5.14(d).

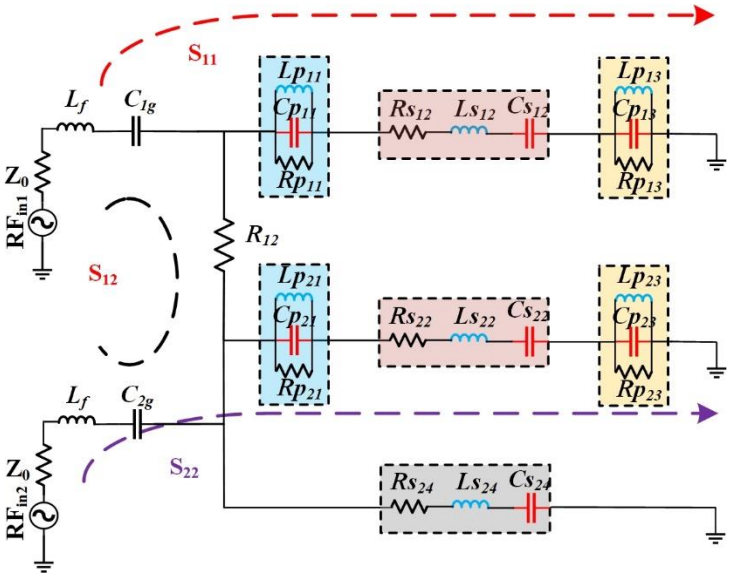

(a)

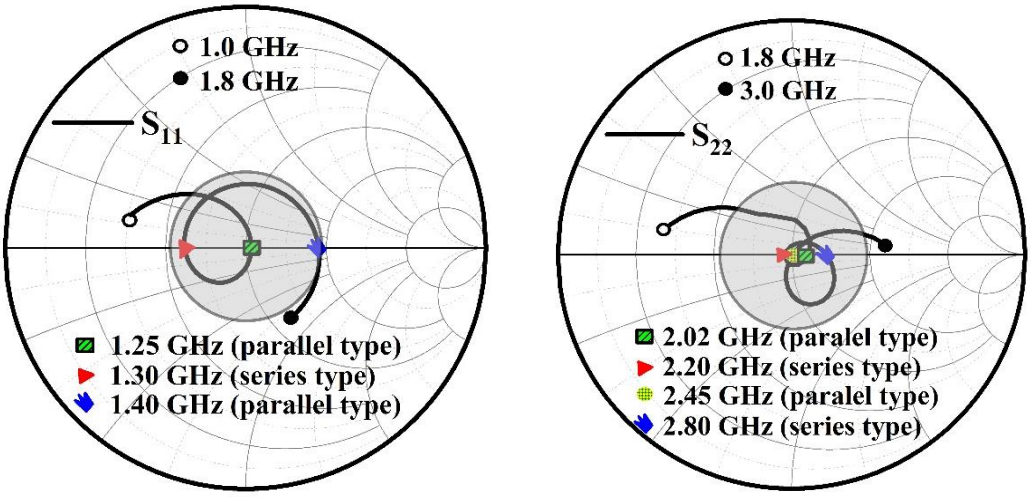

(b)

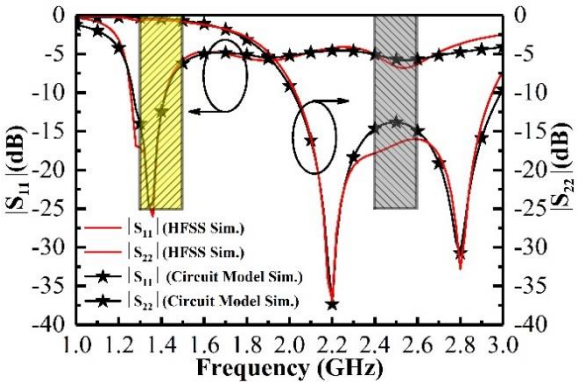

(c)

Parameters symbols and values					
Resistor	**(Ω)**	**Inductor**	**nH**	**Capacitor**	**pF**
Rp11	51.9	*Lp11*	0.6	*Cp11*	20.0
Rp21	59.0	*Lp21*	3.3	*Cp21*	25.0
Rs12	35.6	*Ls12*	0.5	*Cs12*	3.3
Rs22	45.0	*Ls22*	5.7	*Cs22*	1.2
Rp13	95.0	*Lp13*	1.3	*Cp13*	3.9
Rp23	51.0	*Lp23*	1.2	*Cp23*	3.1
Rs24	71.5	*Ls24*	8.2	*Cs24*	0.5
R12	865	*Lf*	0.5	*C1C, C2C*	18.6, 4.3

(d)

Fig. 5.13: (a) Equivalent circuit of the proposed antenna. (b) Smith chart display of impedance. (c) Comparison of S-parameters from full-wave and circuit simulations. (d) Corresponding lumped element values.

5.3 Measured Results and Discussion

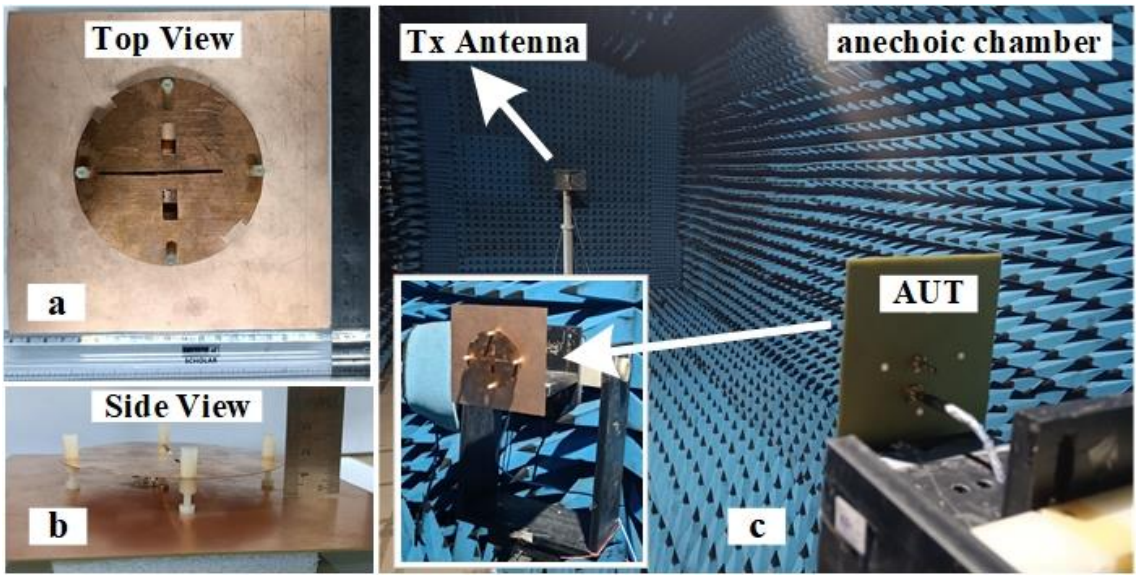

Fig. 5.14: Photographs of the proposed antenna: (a) Top view, (b) side view, and (c) measurement setup.

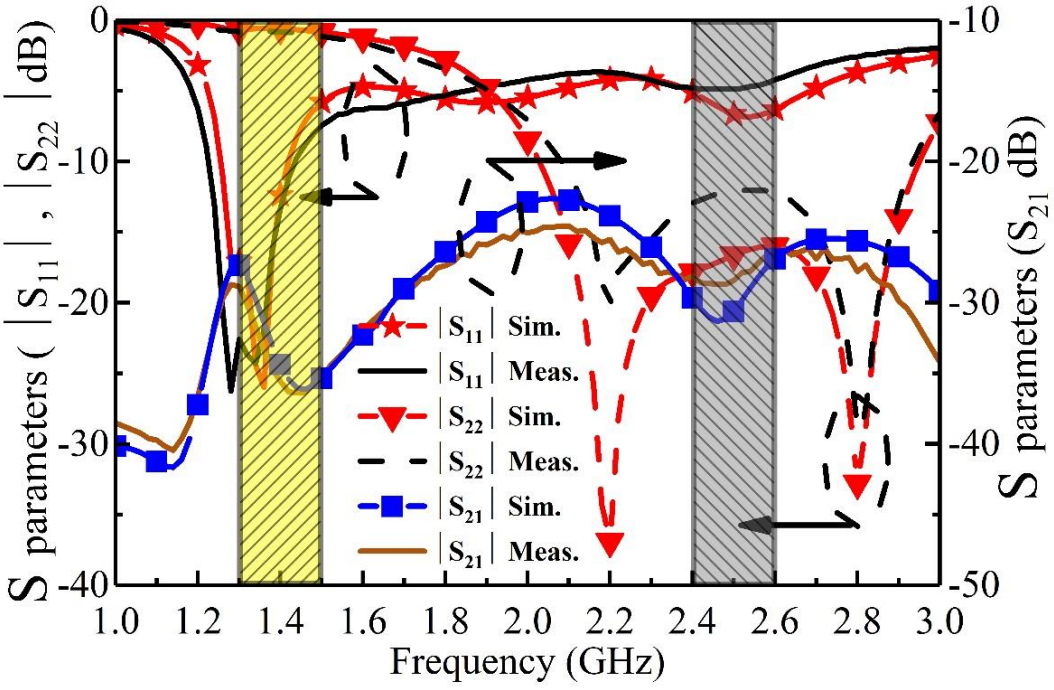

Fig. 5.15: Simulated and measured S-parameters of the proposed antenna.

The proposed suspended plate antenna prototype underwent meticulous fabrication, accompanied by a comprehensive set of measurements to assess its performance. S-

parameters were measured utilizing the Anritsu MS2038C Vector Network Analyzer, and far-field measurements were conducted within an anechoic chamber. Fig. 5.14 illustrates the antenna prototype, showcasing the top view (Fig. 5.14 a), side view (Fig. 5.14 b), and the overall measurement setup (Fig. 5.14 c).

To assess the efficacy of the proposed antenna, Fig. 5.15 presents a comparative analysis of simulated and measured S-parameters. For Port 1, simulated results reveal an impressive impedance bandwidth (IBW) of 1.26 to 1.42 GHz, covering 11.42% of the WMTS band. The measured results closely align with the simulations, demonstrating an IBW of 1.23 to 1.44 GHz with a fractional bandwidth (FBW) of 15.00% within the WMTS band. Similarly, for Port 2, simulated IBW spans from 2.03 to 2.95 GHz, achieving an outstanding FBW of 37.55% corresponding to the ISM band. The measured results for Port 2 showcase an IBW of 2.08 to 2.93 GHz with an FBW of 34.69% for the ISM band. Remarkably, the measured and simulated results exhibit excellent alignment. Furthermore, |S21| measurements reveal exceptional performance, with the measured value reaching -30 dB for the WMTS band and -25 dB for the ISM band.

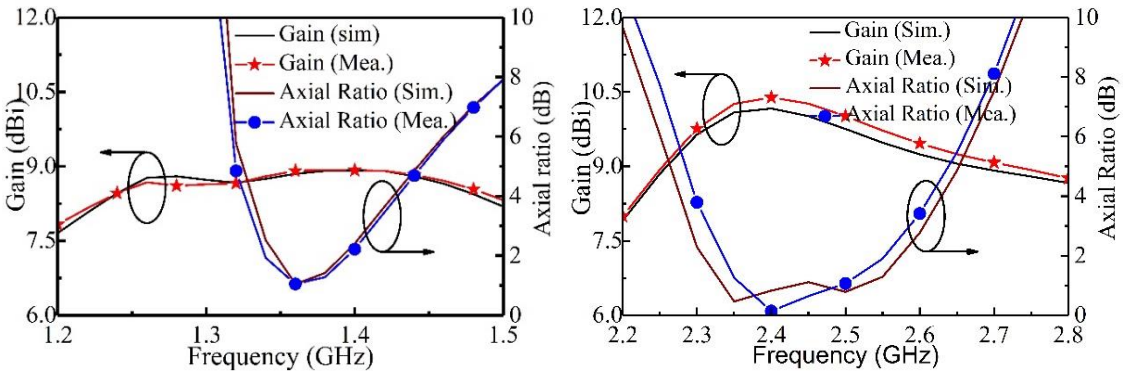

Fig. 5.16: Comparison between simulated and measured axial ratio (AR) and peak realized gain.

Fig. 5.16 provides a comprehensive comparison between simulated and measured axial ratio (AR) and peak realized gain at the broadside. The measured 3 dB AR bandwidths are

noteworthy, spanning 5.7% (1.33–1.41 GHz) for the WMTS band and 11.0% (2.32–2.59 GHz) for the ISM band. Simulated results closely match the measured data, showing AR bandwidths of 5.0% (1.34–1.41 GHz) for the WMTS band and 13.0% (2.29–2.61 GHz) for the ISM band. Additionally, the measured peak realized gains at the broadside are impressive, reaching 8.8 dBi for the lower band (WMTS) and 10.5 dBi for the higher band (ISM).

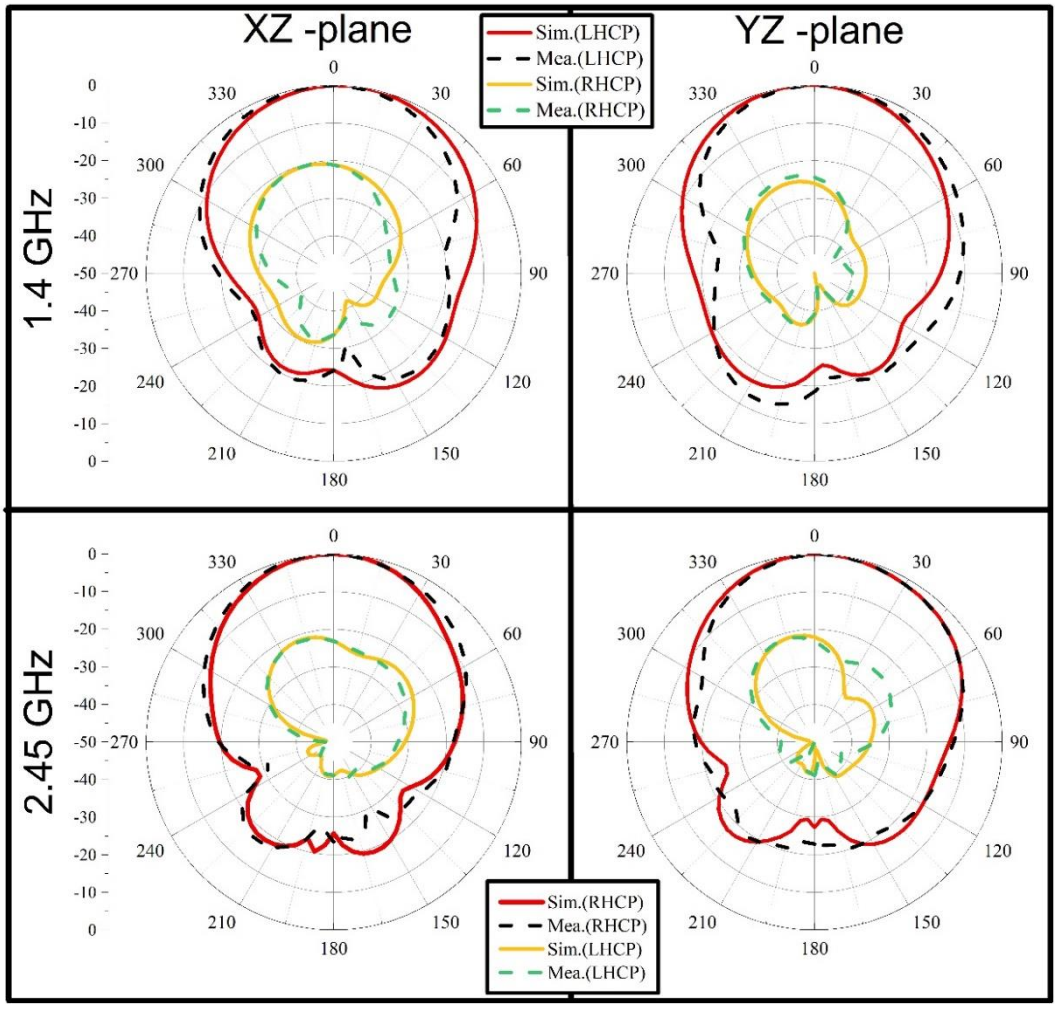

Fig. 5.17: Comparison of simulated and measured normalized radiation patterns in the XZ- and YZ-planes at 1.4 GHz and 2.45 GHz.

Fig. 5.17 provides a detailed comparison of simulated and measured normalized radiation patterns in the XZ- and YZ-planes at 1.4 GHz and 2.45 GHz, when fed by Port 1 and Port 2. When Port 1 is excited, Port 2 is terminated by a 50-ohm load, and vice versa.

Remarkably, at both frequencies, the measured ratio of co-to-cross-polarization radiation levels exceeds 20 dB in both planes for the broadside direction, while the front-to-back ratio remains consistently better than 15 dB.

Table 5.2 offers a comprehensive performance comparison of the proposed dual-band dual-sense antenna with other reported dual-band circularly polarized antennas.

The proposed dual-band antenna at 1.4 GHz and 2.45 GHz offers advantages over referenced bands [80, 82-86, 89] for bio-telemetry applications. Demonstrating wider impedance and axial ratio bandwidths (12.85% / 34.6% for impedance, 5.7% / 11.0% for axial ratio) surpasses references [80, 82-86], attributed to balanced current distribution from slot modifications. While the proposed antenna exhibits peak gains of 8.9 dBi and 10.15 dBi, its good cross-polarization discrimination (-20.4 dB / -15.5 dB) and remarkably compact size (0.16 λ^2) make it a compelling candidate for bio-telemetry applications.

Table 5.2: Comparison between the proposed DBDS CP antenna

Ref.	**Frequency (GHz)**	**Size (λ_0^2)**	**Impedance BW (%)**	**AR BW (%)**	**Peak Gain**	**XPD (dB)**
[80]	2.42(LHCP)/ 2.68(RHCP)	2.17	3.3/2.6	0.9/0.3	11.7/11.8	-18.6/-14.5
[82]	4.4(RHCP)/ 6.44(LHCP)	0.5	13.8/10.0	1.8/3.4	10.22/10.72	NA
[83]	2.55(RHCP)/ 3.53(LHCP)	0.2	NA	27.45/7.1	2.5	-18
[84]	1.93(RHCP)/ 2.5(LHCP)	0.11	2.64/18.03	3.16/5.06	1.4	NA
[85]	2.40(RHCP)/ 3.50(LHCP)	0.96	21.2/9.8	2.9/1.7	7.7/7.4	-16
[86]	0.84(RHCP/ 0.92(LHCP)	0.25	2.99/2.72	1.07/1.19	4.5	NA
[89]	5.0(RHCP)/ 8.0 (LHCP)	2.64	NA	23.5/24.2	12.0 /13.6	NA
proposed	1.4(RHCP)/ 2.45(LHCP)	0.16	12.85 /34.6	5.7/11.0	8.9/10.15	-20.4/-15.5

5.4 Communication Link Setup and Measurement

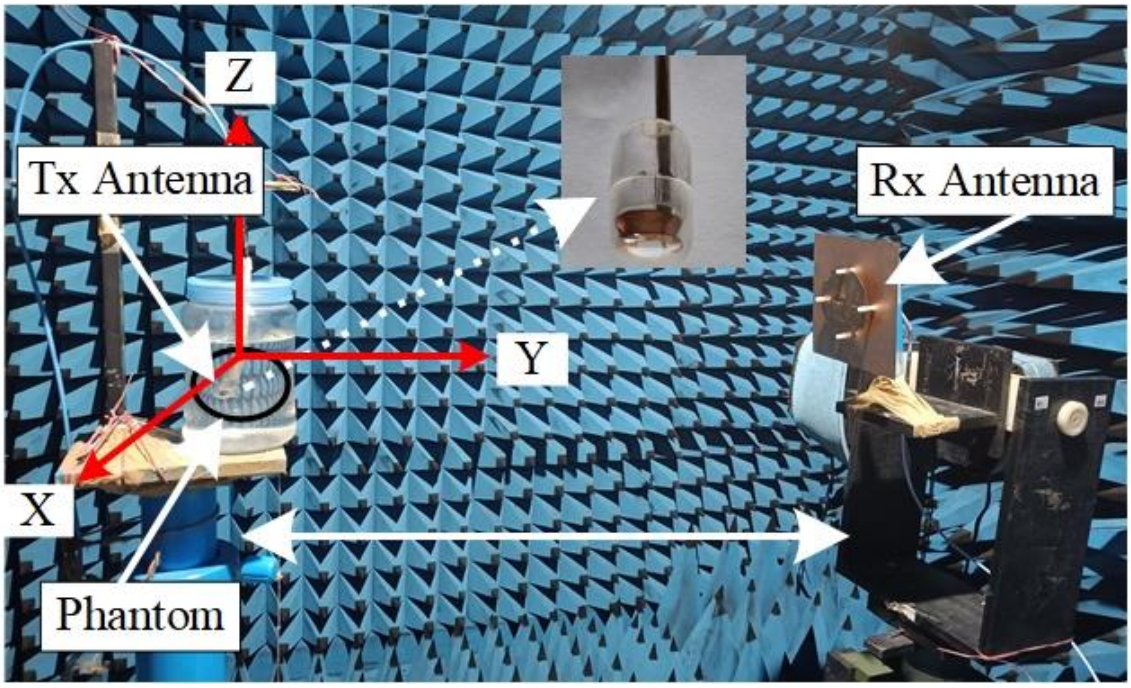

Fig. 5.18: Communication link measurement setup between the DBDS CP antenna and the implantable antenna.

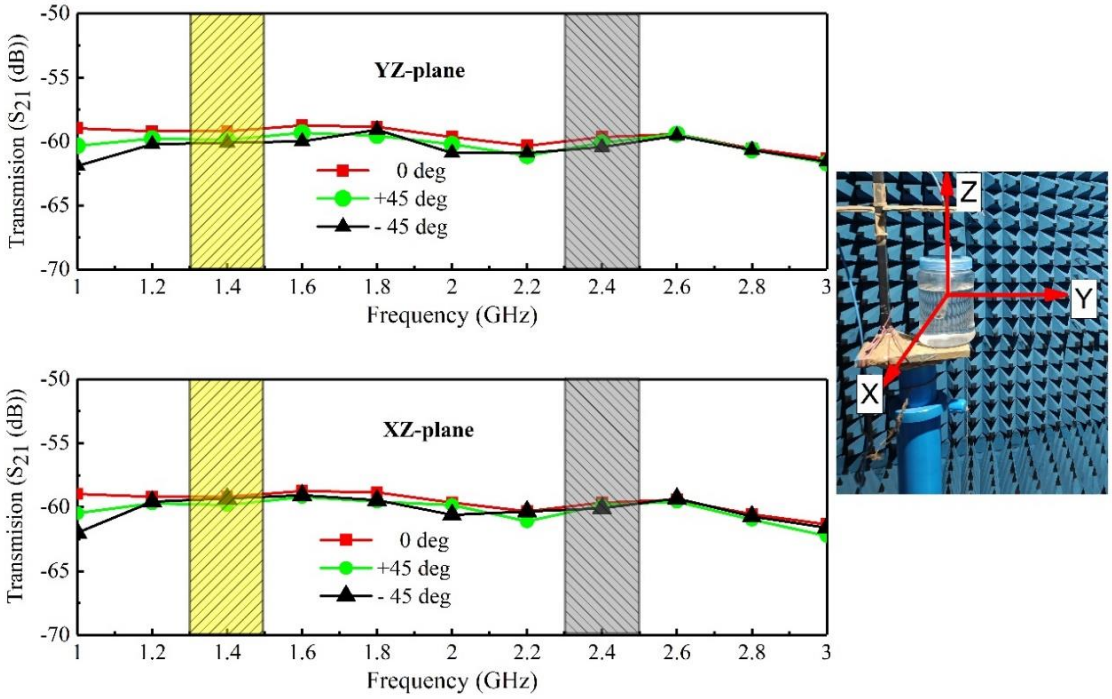

Fig. 5.19: Transmission coefficients (S_{21} (dB)) measurements between the implantable antenna and the proposed DBDS CP antenna: (a) YZ-plane and (b) XZ-plane orientation.

To evaluate the efficacy of the proposed dual-band dual-sense circularly polarized suspended plate antenna with an L-probe feed for wireless communication in biotelemetry, a comprehensive communication link measurement was conducted, as depicted in Fig. 5.18, using the ingestible antenna.

The ingestible antenna operates seamlessly within two distinct frequency bands—the Wireless Medical Telemetry Service (WMTS) bands (1.395 – 1.400 GHz and 1.427 – 1.432 GHz) and the Industrial, Scientific, and Medical (ISM) band (2.48 GHz - 2.4 GHz). Housed within a compact capsule measuring approximately 11 mm x 26 mm, the antenna exhibits a nearly isotropic radiation pattern. Notably, its design ensures durability to withstand the challenging environment of the gastrointestinal tract. A comprehensive evaluation and thorough assessment of the ingestible antenna's performance are detailed in [124].The suspended plate antenna is meticulously engineered to operate cohesively within the same two frequency bands, ensuring a seamless and reliable communication link with the ingestible antenna.

To gauge the performance of the communication link between the ingestible antenna and the suspended plate antenna, the ingestible antenna was immersed in a body tissue liquid phantom and connected to port 1 of a Vector Network Analyzer (VNA). The dual-band dual-sense circularly polarized suspended plate antenna, positioned 2 meters away from the body tissue liquid container, was connected to port 2 of the VNA.

A series of experiments were conducted to assess the transmission coefficients (S_{21} (dB)) between the two antennas under various orientation conditions. The transmission coefficient, a crucial parameter characterizing the link's efficiency, was measured to quantify the proportion of power transferred from the ingestible antenna to the suspended plate antenna, providing a robust indication of the overall effectiveness of the communication link.

The transmitting antenna underwent controlled rotation in the yz-plane and xz-plane, as illustrated in Fig. 5.19(a) and 5.19(b), respectively. An analysis of S_{21} reveals that the received power for the in-body capsule link remains consistently stable across different rotation angles for both frequencies, indicating the capsule antenna's remarkable stability. The S_{21} variation is observed to be less than 3 dB for all rotations in both planes at both frequencies, ranging from 0.8 μW to 2.4 μW. This performance attests to the circularly polarized nature of the antenna, significantly enhancing the link's robustness to capsule orientation changes.

After conducting two sets of communication link studies, it becomes evident that the proposed circular polarization antenna design serves as a pivotal enabler in this communication link, effectively addressing the dynamic orientation changes of the ingestible device within the human body. By ensuring consistent signal reception regardless of orientation, circular polarization enhances the robustness and reliability of the communication link, a crucial factor given the unpredictable conditions within the digestive tract.

5.5 Summary

This chapter introduces a dual-band, dual-sense (DBDS) circularly polarized high gain suspended plate antenna with an L-probe feed tailored for bio-telemetry. Operating seamlessly within WMTS bands (1.395–1.400 GHz, 1.427–1.432 GHz) and the ISM band (2.48–2.40 GHz), the design intricacy was meticulously optimized for exceptional performance.

Integration of double L-shaped strips and electromagnetic coupling with the center slot results in a commendable impedance bandwidth, ensuring robust communication. Measured results closely align with simulated values, validating the reliability of our dual-

band design. For WMTS, the antenna achieves a -10 dB reflection coefficient bandwidth of 15 % (1.44-1.23 GHz), and the ISM band exhibits a bandwidth of 34.69% (2.93-2.08 GHz), confirming its proficiency in dual-band bio-telemetry applications.

Measured 3-dB axial ratio bandwidths of 5.7% (1.41-1.33 GHz) for WMTS and 11.0% (2.59-2.32 GHz) for ISM confirm circular polarization characteristics vital for reliable communication. Peak realized gains of 8.9 dBi and 10.15 dBi underscore the antenna's exceptional radiation efficiency.

Radiation pattern measurements unveil directional properties, characterized by low cross-polarization and favourable front-to-back radiation ratios. These contribute to the antenna's outstanding performance in impedance bandwidth, axial ratio bandwidth, peak realized gain, and radiation pattern.

In conclusion, our proposed dual-band dual-circularly polarized suspended plate antenna, with its innovative design and validated metrics, positions itself for bio-telemetry in WMTS and ISM bands. Validation with a dual-band ingestible antenna demonstrates success in reducing polarization mismatch, maintaining reliable communication links, enhancing its potential in dual-band bio-telemetry systems. The forthcoming chapter-6 aims to encapsulate these achievements, offering insightful conclusions and future directions in the pursuit of enhancing bio-telemetry systems.